AIAA JOURNAL
Vol. 46, No. 4, April 2008

Numerical Modeling of Sound Diffraction at a Half-Plane Trailing Edge

Mariano Genito* and Damiano Casalino†
Italian Aerospace Research Center, I-81043 Capua, Italy

DOI: 10.2514/1.32047

The problem of sound propagation in the presence of a rigid semi-infinite plate and a double-stream sheared mean flow is solved numerically by means of a linearized Lilley's equation. This is discretized in the frequency domain by using a Green's function discretization scheme leading to a very efficient numerical method. It is demonstrated that the present approach is able to tackle the edge diffraction problem without any additional treatment of the vortex sheet and that it provides results that are in close agreement with the analytical solution for a uniform mean flow. In addition it is shown that the results obtained by considering a piecewise constant mean flow and a mixing layer mean flow compare favorably with the solutions obtained by solving the linearized Euler equations using a discontinuous Galerkin method.

I. Introduction

THE sound scattering by a semi-infinite hard plate is a model problem for the propagation of acoustic waves in the presence of a diffracting edge. Numerical methods able to treat this kind of problem can be applied to the calculation of sound propagation in real configurations, such as the bypass duct nozzle of a turbofan engine [1] and the high-lift device system of a wing [2,3]. Various analytical techniques have been developed in the past to provide a qualitative and quantitative description of the problem. These solutions still constitute a severe benchmark for numerical methods. The first analytical solution was put forward by Sommerfeld [4] who solved the Helmholtz equation in the absence of flow. Later on Noble [5] addressed the problem by using the Wiener–Hopf technique. This approach has become a standard solution technique for complex aeroacoustic problems involving semi-infinite configurations. When a mean flow, even if uniform, is present, the analytical solutions based on the acoustic velocity potential are no longer valid, because the impinging acoustic wave induces the formation of a vortical wake at the edge. The problem can be tackled by solving the linearized Euler equations (LEE) that support also vorticity disturbances [6]. To avoid the solution of a system of equations, several authors have supposed that the vorticity shed from the trailing edge is confined within an infinitesimal vortex sheet parallel to the mean flow [7–9]. The coupling between the acoustic pressure and vorticity fields is obtained by imposing the continuity of pressure and normal velocity across the vortex sheet and by forcing the acoustic perturbation (vorticity free) equation to satisfy the Kutta condition at the edge. This solution, however, is only valid in a low-frequency approximation, when the acoustic wavelength is larger than the thickness of the plate. Moreover, the validity of the solution is restricted to a uniform or piecewise uniform flow.

Following Candel [10], who argued that the problem of sound diffraction is much more conveniently expressed in terms of acoustic pressure that is continuous across the vortex sheet, a numerical method [11] based on the solution of a homogeneous linearized Lilley's equation is used in this paper to solve the half-plane diffraction problem. The linearized Lilley's equation is a third-order wave equation for the acoustic perturbation, whose nonhomogeneous counterpart is typically used as an acoustic analogy equation in the framework of jet noise prediction [12–14]. The solution of the linearized Lilley's equation does not require a vortex sheet model or the imposition of a Kutta condition. In addition, this equation is also valid if the mean flow is a unidirectional transversely sheared rotational flow. As a consequence, the present numerical method has a wider applicability range than analytical methods, and it is cheaper than a LEE-based approach. In fact, it is based on the efficient solution of a scalar equation in the frequency domain by using a Green's function discretization (GFD) scheme [15,16]. The numerical approach is verified through comparisons against analytical solutions for the quiescent and uniform medium cases. A time-domain code solving the LEE system by means of a discontinuous Galerkin method (LEE-DGM), verified against the same analytical solutions, is used as a reference solution for the other cases. In [17] the same frequency-domain approach has been used to compute the diffraction of a spinning duct mode by the open end of a duct with a centerbody. Numerical results are then compared with the Wiener–Hopf analytical solution recently obtained by Gabard and Astley [18], showing good agreement.

The layout of the paper is as follows. In Sec. II the governing equations are presented with a discussion on their applicability limits. A brief presentation of Candel's analytical solution [10] is given in Sec. III. Section IV is devoted to the description of the numerical methods employed, with particular attention to the boundary conditions and to the edge representation. In Sec. V numerical results for a grazing plane wave that propagates in a quiescent, uniform, piecewise constant, and nonuniform flow are presented. The choice of the parallel direction of propagation has been dictated by the necessity of clearly showing the effects of refraction on the diffracted wave, without contamination by the reflected field. The main conclusions of this study are finally drawn in Sec. VI.

II. Governing Equations

Starting from the Navier-Stokes equations and neglecting the viscous terms it is possible to obtain the Euler system of equations written in terms of primitive variables (density ρ, velocity $\mathbf{v}$ and pressure p):

$$\frac{\mathrm{D}\rho}{\mathrm{D}t} + \rho\nabla\cdot\mathbf{v} = 0 \qquad \frac{\mathrm{D}\mathbf{v}}{\mathrm{D}t} + \frac{\nabla p}{\rho} = 0 \qquad \frac{\mathrm{D}p}{\mathrm{D}t} + \rho c^2\nabla\cdot\mathbf{v} = 0 \tag{1}$$

Presented as Paper 3503 at the 13th AIAA/CEAS Aeroacoustics Conference, Rome, 21–23 May 2007; received 9 May 2007; revision received 29 October 2007; accepted for publication 30 October 2007.

*Research Engineer, Rotorcraft Aerodynamics and Aeroacoustics Laboratory, CIRA.

†Senior Research Engineer, Rotorcraft Aerodynamics and Aeroacoustics Laboratory, CIRA. Member AIAA.

where c is the sound speed and the total derivative is defined as

$$\frac{\mathrm{D}}{\mathrm{D}t} = \frac{\partial}{\partial t} + \mathbf{v}\cdot\nabla \tag{2}$$

Following Lilley [19], it is possible to rearrange the Euler equations in the form of a third-order equation:

$$\frac{\mathrm{D}}{\mathrm{D}t}\left[\frac{\mathrm{D}^2\Pi}{\mathrm{D}t^2} - \frac{\partial}{\partial x_j}\left(c^2\frac{\partial \Pi}{\partial x_j}\right)\right] + 2\frac{\partial v_k}{\partial x_j}\frac{\partial}{\partial x_k}\left(c^2\frac{\partial \Pi}{\partial x_j}\right) = -2\frac{\partial v_j}{\partial x_k}\frac{\partial v_i}{\partial x_j}\frac{\partial v_k}{\partial x_i} \tag{3}$$

where $\Pi = 1/\gamma\,\ell_n\, p/p_0$; γ is the ratio of the specific heats, and p_0 is a reference pressure.

Supposing that the thermodynamic and kinetic variables can be expressed as the sum of a mean-flow quantity (denoted with an overline) and a perturbation (denoted with a prime), which is 1 order of magnitude smaller than the corresponding mean-flow quantity, it is possible to obtain from Eq. (1) the LEEs:

$$\begin{aligned}
\frac{\bar{\mathrm{D}}\rho'}{\mathrm{D}t} + \bar{\rho}\nabla\cdot\mathbf{v}' + \mathbf{v}'\cdot\nabla\bar{\rho} + \rho'\nabla\cdot\bar{\mathbf{v}} &= S_\rho \\
\frac{\bar{\mathrm{D}}\mathbf{v}'}{\mathrm{D}t} + \frac{\nabla p'}{\bar{\rho}} + \mathbf{v}'\nabla\bar{\mathbf{v}} &= S_{\mathbf{v}} \\
\frac{\bar{\mathrm{D}}p'}{\mathrm{D}t} + \bar{\rho}\bar{c}^2\nabla\cdot\mathbf{v}' + \mathbf{v}'\cdot\nabla\bar{p} + (\rho'\bar{c}^2 + \bar{\rho}(c^2)')\nabla\cdot\bar{\mathbf{v}} &= S_p
\end{aligned} \tag{4}$$

and from Eq. (3) the linearized Lilley's equation for the quantity $\Pi' = 1/\gamma p'/p_0$:

$$\frac{\bar{\mathrm{D}}}{\mathrm{D}t}\left[\frac{\bar{\mathrm{D}}^2\Pi'}{\mathrm{D}t^2} - \frac{\partial}{\partial x_j}\left(\bar{c}^2\frac{\partial \Pi'}{\partial x_j}\right)\right] + 2\frac{\partial \bar{v}_k}{\partial x_j}\frac{\partial}{\partial x_k}\left(\bar{c}^2\frac{\partial \Pi'}{\partial x_j}\right) = S_{\Pi'} \tag{5}$$

In Eqs. (4) and (5) use of the mean-flow Lagrangian derivative:

$$\frac{\bar{\mathrm{D}}}{\mathrm{D}t} = \frac{\partial}{\partial t} + \bar{\mathbf{v}}\cdot\nabla \tag{6}$$

has been done, and the higher-order terms have been gathered in the form of source terms at the right-hand side. Indeed, the source term $S_{\Pi'}$ in Eq. (5) is of higher order compared to Π' only if the mean flow is a unidirectional transversely sheared flow. In the present work the aeroacoustic generation problem is not addressed, because the noise excitation is only prescribed via boundary conditions. In addition, the mean velocity is parallel to the flat plate and varies only along the normal direction. Therefore, only the homogeneous wave operator is considered. The perturbation velocity appearing in Eq. (4) can be thought of as the sum of the velocity due to the acoustic, vortical, and entropy modes present in the field, that is, $\mathbf{v}' = \mathbf{v}'_{\mathrm{ac}} + \mathbf{v}'_{\Omega} + \mathbf{v}'_s$. Because the acoustic field is irrotational, it is possible to introduce the potential of the acoustic velocity $\nabla\phi = \mathbf{v}'_{\mathrm{ac}}$, which is related to the acoustic pressure via the equation:

$$p' = -\bar{\rho}\left(\frac{\partial\phi}{\partial t} + \bar{\mathbf{v}}\cdot\nabla\phi\right) \tag{7}$$

Using this definition it is possible to derive from Eq. (4) the following equation:

$$\bar{c}^2\nabla^2\phi - \frac{\partial^2\phi}{\partial t^2} - 2\bar{\mathbf{v}}\cdot\frac{\partial\nabla\phi}{\partial t} - \bar{\mathbf{v}}\cdot\nabla(\bar{\mathbf{v}}\cdot\nabla\phi) - \nabla\left(\frac{\bar{\mathbf{v}}^2}{2}\right)\cdot\nabla\phi - (\gamma-1)\left(\frac{\partial\phi}{\partial t} + \bar{\mathbf{v}}\cdot\nabla\phi\right)\nabla\cdot\bar{\mathbf{v}} = S_{\Omega,s} \tag{8}$$

where the right-hand side is a source term accounting for the effects of vorticity and entropic disturbances on the acoustic mode.

It can be stated that for a generic aeroacoustic problem the acoustic pressure can be obtained by solving the complete set of linearized Euler equations (4), the linearized Lilley's equation (5), or the acoustic potential equation (8). However, due to the boundary conditions, the latter approach is not fully equivalent to the others. Let us consider, for example, the slip condition $\mathbf{v}'\cdot\mathbf{n} = 0$, where $\mathbf{n}$ is the unit normal vector to the wall. This provides the following wall condition for the acoustic potential:

$$\frac{\partial\phi}{\partial n} = -\mathbf{v}'_{\Omega}\cdot\mathbf{n} - \mathbf{v}'_s\cdot\mathbf{n} \tag{9}$$

From Eq. (9) it is clear that the solution of the acoustic mode can be pursued only if the vorticity and the entropy modes are known. In other words the use of Eq. (8) requires the explicit modeling of the vorticity and entropy modes. A common strategy used in the analytical solution of a diffraction problem in the presence of a semi-infinite plate or a semi-infinite duct is to use a low-frequency approximation, according to which the vorticity is confined in a harmonic wake that is frozenly convected by the mean flow. The magnitude of the wake is determined by imposing a Kutta condition at the edge, which is equivalent to a pressure continuity condition across the wake. In this way the problem is restricted to a scalar equation that can be conveniently solved by using the Wiener–Hopf technique. The same approach could be used in a numerical approach, but two problems arise: a vortex sheet model is required, and it is not possible to tackle nonuniform mean flows.

To overcome these problems, while containing the computational costs, a numerical method based on a frequency-domain solution of the homogeneous counterpart of Eq. (5) is presented. In the case of a unidirectional transversely sheared flow, this equation is fully equivalent to the LEE system and does not need any explicit treatment of the wake. A similar approach has been used by Candel [10], who obtained a solution for the uniform flow case by solving a second-order wave equation for the acoustic pressure, which can be obtained form Eqs. (4) or (5) under the hypothesis of uniform mean flow.

III. Analytical Solution

The problem under investigation is the scattering of a plane wave by a semi-infinite plate with edge. The flow on both sides of the plate is subsonic and with positive direction $0 \le \bar{M} = \bar{u}/\bar{c} < 1$. Because of the harmonic nature of the incident plane wave, the solution can be conveniently expressed in the frequency domain. If ω is the radian frequency and $k = \omega/\bar{c}$ is the acoustic wave number, a generic quantity is expressed as $\phi = \hat{\phi}^{-i\omega t}$, where the hat denotes complex amplitude.

For this problem, Noble [5] obtained a solution in the absence of flow by solving the acoustic potential wave equation (Helmholtz equation). For this case the produced vorticity remains confined at the edge and the Helmholtz equation is therefore able to predict the diffracted sound field, provided that the singularity of the velocity potential at the edge is properly removed. The solution obtained by Noble and reported by Candel [10] expresses the acoustic field generated by the impinging acoustic wave by means of the complex Fresnel integral F in cylindrical coordinates (r,θ) centered at the edge:

$$\hat{\phi}_0(r,\theta,k,\Theta) = \frac{e^{-i(kr+\pi/4)}}{\sqrt{\pi}}\left\{e^{-i\cos(\theta-\Theta)}F\left[-\sqrt{2kr}\cos\left(\frac{\theta-\Theta}{2}\right)\right] + e^{-i\cos(\theta+\Theta)}F\left[\sqrt{2kr}\cos\left(\frac{\theta+\Theta}{2}\right)\right]\right\} \tag{10}$$

where Θ is the plane wave incidence angle and the complex Fresnel integral is defined as

$$F(v) = \int_v^{+\infty} e^{iu^2}\,\mathrm{d}u \tag{11}$$

From Eq. (7) follows that the complex amplitude of the acoustic pressure is simply given by

$$\hat{p}'_0 = i\bar{\rho}\,\bar{c}\,k\hat{\phi}_0 \tag{12}$$

Starting from Noble's solution, Candel argued that, because the wave equation written in terms of pressure is decoupled by the evolution of the vortical mode, the solution for the uniform flow case can be obtained from Eq. (10) by simply applying a Prandtl–Glauert transformation. Hence, the uniform flow solution is given by

$$\hat{p}'(x, y, k, \Theta, \bar{M}) = e^{-ik_1 \bar{M} x_1} \hat{p}'_0(x_1, y, k_1, \Theta_1) \tag{13}$$

where superscripts 1 denote Prandl–Glauert transformed quantities, say

$$\begin{aligned} x_1 &= x/\sqrt{1-\bar{M}^2} \qquad k_1 = k/\sqrt{1-\bar{M}^2} \\ \cos\Theta_1 &= (\cos\Theta - \bar{M})/(1-\bar{M}\cos\Theta) \end{aligned} \tag{14}$$

A simple interpretation of Eq. (13) can be drawn by subtracting from the total field the incident and reflected fields. The remaining diffracted field $\hat{p}'_d$ can be approximated in the far-field limit $kr \gg 1$ by a two-dimensional monopole with nonuniform directivity[10]:

$$\hat{p}'_d \approx \frac{e^{i(k_1 r_1 + \pi/4)}}{\sqrt{2\pi k_1 r_1}} D(\theta_1, \Theta_1) \tag{15}$$

If the impinging plane wave has a direction of propagation parallel to the plate, then the reflected wave vanishes. In this case the acoustic field is the sum of an incident plane wave and the field generated by a point source located at the edge and immersed in a uniform flow.

IV. Discretization Method

To highlight the behavior of the diffraction field in all the numerical solutions, a plane wave parallel to the plane has been considered. For the quiescent case a wave number $k = 6.28$ is considered, resulting in a unitary wavelength used as reference length throughout the paper. For the other cases, if not otherwise specified, the same wave number is used. The thermodynamic mean-flow quantities are nondimensionalized by using the sound speed and density of a reference flow condition, resulting in unitary nondimensional speed of sound and density. Numerical solutions have been carried out by using both a frequency-domain (Lilley–GFD) and a time-domain (LEE–DGM) approach. For both the Lilley–GFD and LEE–DGM computations, a two-dimensional Cartesian grid with a uniform spacing equal to 0.1 is used, resulting in 10 points per wavelength for the quiescent case. The plate, as in the analytical solution, has an infinitesimal thickness, and its projection onto the computational domain is represented by two coincident lines that are topologically disconnected. The x axis of the coordinate system is parallel to the plate and the y axis is normal to it. The edge coordinates in that system are $(x_E, y_E) = (10, 10)$.

The LEE–DGM code solves the LEE system (4) by means of a quadrature-free discontinuous Galerkin method [20]. For the present study, a third-order polynomial representation and a third-order Runge–Kutta time-marching scheme have been used. The inflow condition has been imposed by means of a characteristic variables approach [21] and the outflow condition is provided by a perfectly matched layer (PML) method [21] in conjunction with a characteristic outflow condition imposed on the outer boundary of the PML region. The PML extension is equal to 2 and the PML damping constant is equal to 0.3. On the plate the impenetrability condition has been applied, without any special treatment at the edge. In fact, since the DGM collocates the polynomials in the cell centers and does not require the matching at the cell faces, this method is naturally suited to treat a discontinuous field. In this way the singularity of the solution at the edge is automatically treated.

The Lilley–GFD code solves the frequency-domain counterpart of Eq. (5) by means of a GFD method [15,16]. This is a wave-based finite-difference method for unstructured grids. The discretization kernel is based on the use of approximate local solutions of the acoustic problem in order to build a linear combination of free-space Green's functions for the convected Helmholtz equation that can be used as shape functions for the unknowns and their derivatives. This scheme has spectral-like properties allowing one to preserve accuracy up to 3–4 grid points per acoustic wavelength. At the outer boundary a Sommerfeld-type radiation condition for the diffracted field has been imposed because, according to the interpretation given by Candel [10], the diffracted field can be represented as a monopole with nonuniform directivity [Eq. (15)]. Therefore, the radiation condition can be written as

$$\frac{\partial p'}{\partial r} - \mathcal{M} p' = \frac{\partial p'_{\text{inc}}}{\partial r} - \mathcal{M} p'_{\text{inc}} \tag{16}$$

where r denotes the radial direction computed with respect to the edge location, $\mathcal{M} = ik(-M_r + \sqrt{M_r^2 + \beta^2})/\beta^2$ is the so-called Dirichlet-to-Neumann factor, M_r is the mean-flow Mach number projected on the radial direction, β is the Prandtl–Glauert factor, and p'_{inc} is the prescribed acoustic incident field that, in the addressed cases, is nonzero only in the half-plane $y < 0$. Because of the fact that the GFD shape functions are collocated at the grid nodes, a special boundary condition should be imposed at the edge. However, by supposing that the edge is effectively located in the middle of the grid segment downstream of the geometric edge, the problem of the edge condition can be overcome. Hence, by imposing a slip boundary condition with the same normal vector at all points of the plate, the geometric edge included, the solution of the wave equation (5) in the first downstream grid point ensures an implicit (no-modeling) treatment of the edge condition. In a way similar to the time-domain DGM approach the problem of treating the edge singularity has been overcome thanks to the hybrid finite-difference/finite-element properties of the GFD approach.

V. Numerical Results

In this section, the diffraction of a grazing plane wave by the edge of a rigid semi-infinite flat plate is computed for different mean-flow conditions. The edge is located at the point (10, 10), as shown, for instance, in Fig. 4.

A. Quiescent Medium Case

In this section, results obtained for the case $k = 6.28$ and an incident wave of unitary pressure amplitude are compared with the analytical solution (12). Both the frequency-domain (Lilley–GFD) and the time-domain (LEE–DGM) codes correctly reproduce the behavior of the diffracted field, as evident from Fig. 1 where the acoustic pressure along the line $y = 15$ is plotted. For the Lilley–GFD solution, the relative L_2 amplitude and phase errors, defined in [11], are about 7×10^{-3} and 5×10^{-4}, respectively, provided that the analytical solution is computed by considering the effective edge location $x_E + \Delta x/2$.

B. Uniform Mean Flow

Figure 2 shows a comparison between Candel's analytical solution [Eq. (13)] and the Lilley–GFD solution for the plane wave diffraction in the presence of a uniform flow ($\bar{M} = 0.3$). As in the quiescent medium case, the incident plane wave has unitary amplitude and acoustic wave number $k = 6.28$. The real part of the acoustic pressure along two parallel lines one grid segment below ($y = 9.99$) and above ($y = 10.01$) the half-plane is plotted, showing good agreement between the analytical and the numerical solutions. The relative L_0 error of $Re(p')$ along these two lines is about 5% and occurs at an observation angle of 90 deg ($x = 10$, $y = 10.01$).

The same comparison is then carried out for the LEE–DGM simulation as shown in Fig. 3. Also in this case good agreement between numerical results and Eq. (13) is evident, the relative L_0 error not exceeding 5%.

In Fig. 4 the contour plots of the velocity components obtained by using the LEE–DGM approach are shown. It is clearly evident that the time-domain code is able to predict the formation and convection of a vortical wake. In addition, because the velocity component along y is only due to the diffracted field, Fig. 4b confirms that the diffracted field spreads like a monopole, as predicted by Candel [10].

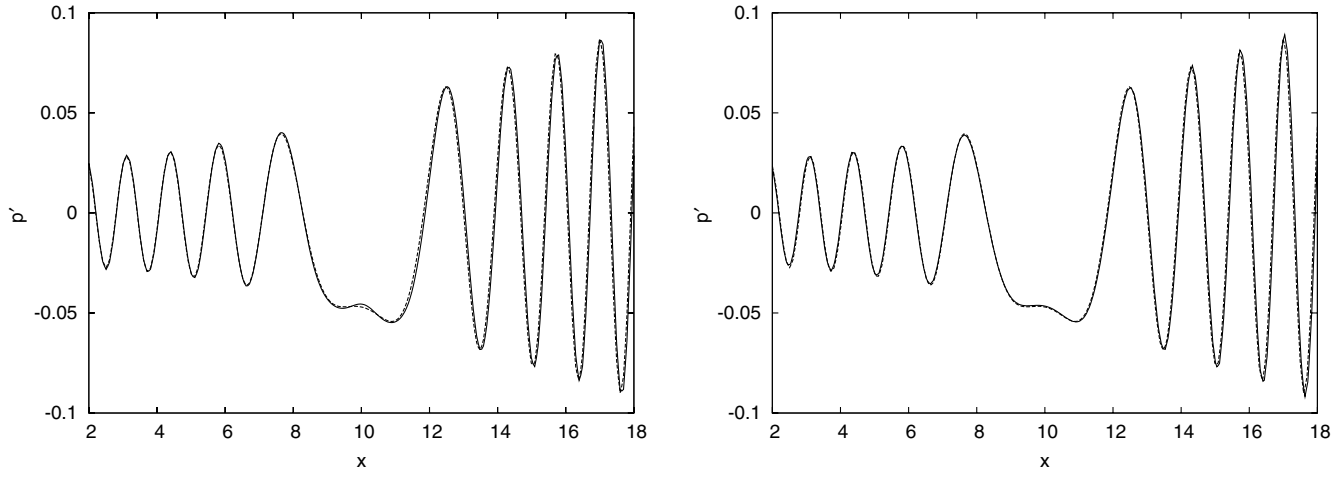

a) Lilley-GFD: Re(p') **b) LEE-DGM: p' at the start of a cycle**

Fig. 1 Quiescent medium case. Comparison between numerical (solid lines) and analytical (dashed lines) solutions.

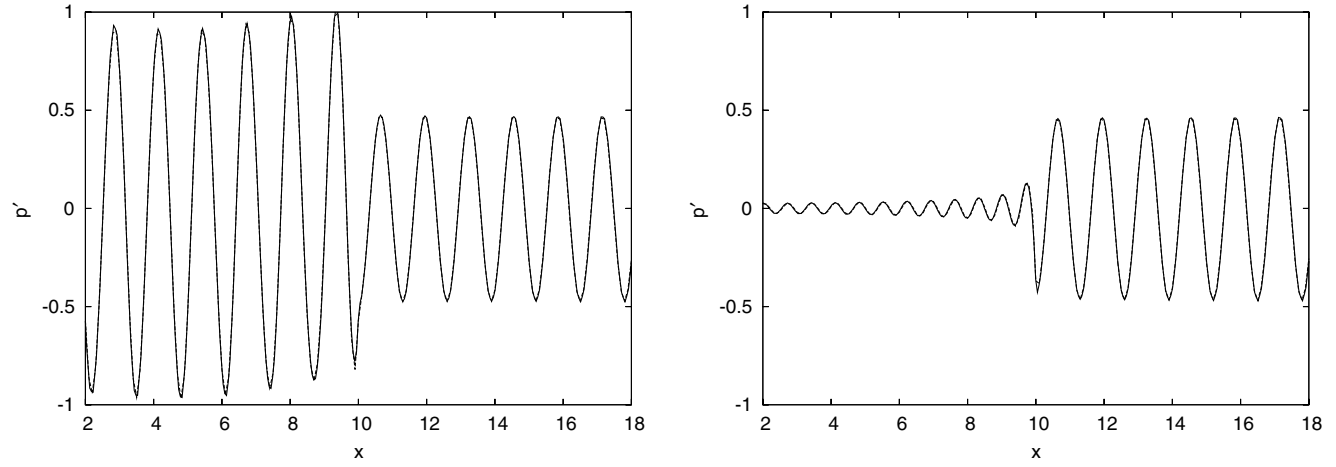

a) y = 9.99 **b) y = 10.01**

Fig. 2 Uniform flow case, $Re(p')$. Comparison between Lilley–GFD (solid lines) and analytical (dashed lines) solutions.

In Fig. 5a the vorticity fluctuation $\omega' = \partial v'/\partial x - \partial u'/\partial y$ along two parallel lines one grid segment below and above the plate is plotted as a function of the distance from the edge divided by the mean-flow Mach number. As expected, a unitary wavelength is exhibited by the vortical wake. In Fig. 5b the x-velocity component along the same lines as a function of the coordinate x divided by the Doppler factor $(1 + \bar{M})$ is plotted. From this figure it is clearly evident that the perturbation velocity is equal to the sum of the

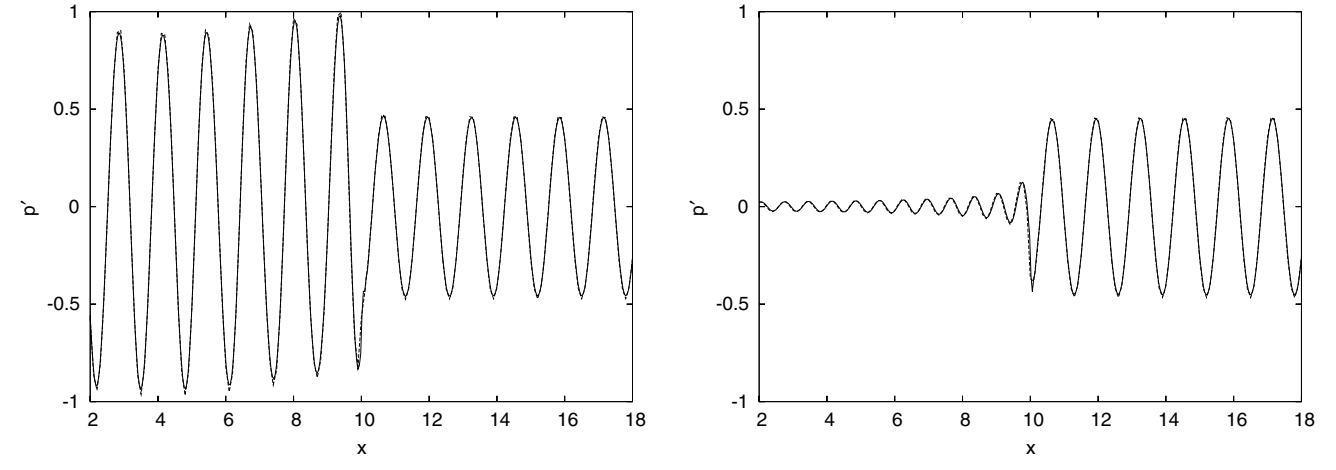

a) y = 9.99 **b) y = 10.01**

Fig. 3 Uniform flow case, p' at the start of a cycle. Comparison between LEE–DGM (solid lines) and analytical (dashed lines) solutions.

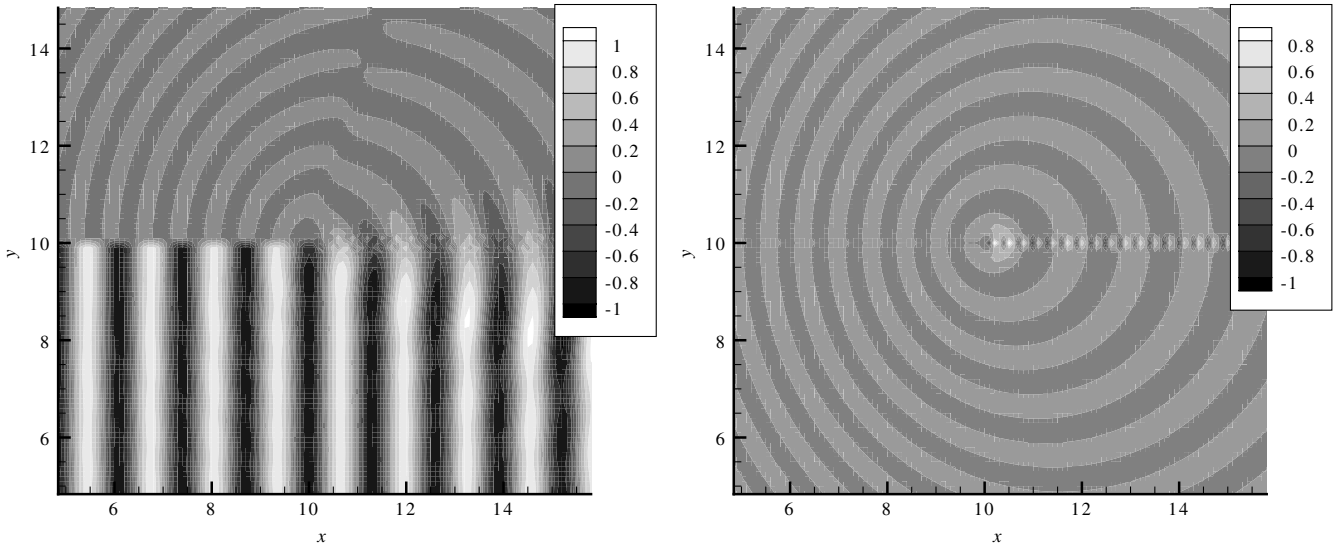

a) Velocity component along *x* **b) Velocity component along *y***

Fig. 4 Uniform flow case. Contour plots of the LEE–DGM solution.

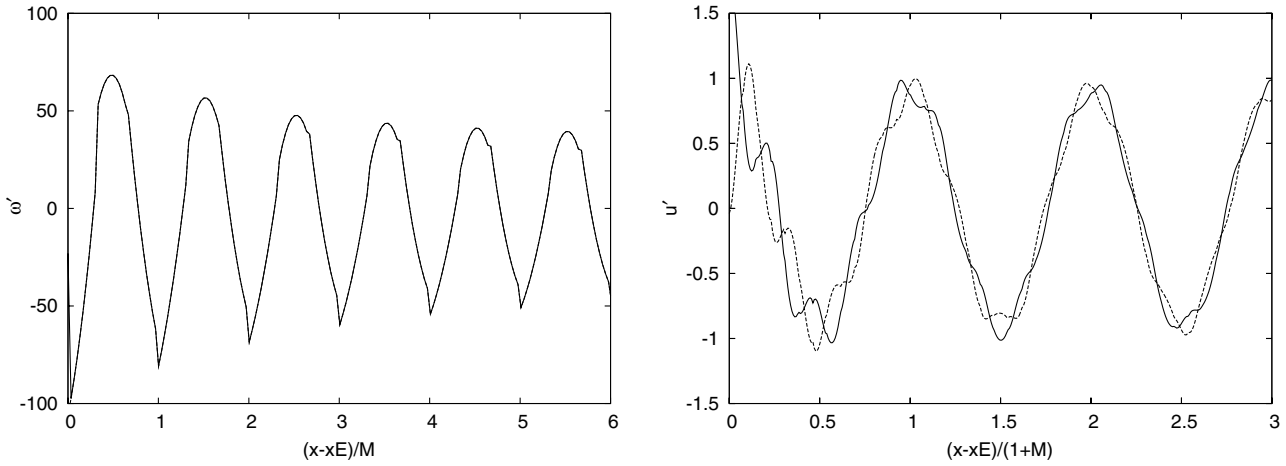

a) Perturbation vorticity **b) Perturbation velocity component along *x***

Fig. 5 Uniform flow case. Line plots of the LEE–DGM solution along the lines $y = 9.99$ (solid lines) and $y = 10.01$ (dashed lines).

acoustic wave of unitary wavelength and the vorticity wave with a shorter wavelength.

As already mentioned, the use of the Lilley's equation does not require the explicit imposition of the Kutta condition, because this equation is decoupled by the equation describing the evolution of the other modes. The use of the acoustic potential wave equation (8), instead, requires the explicit imposition of the Kutta condition and an explicit treatment of the vortex sheet. To evaluate the effects of the Kutta condition on the numerical solution, the same case has been simulated by solving Eq. (8), without any explicit treatment at the edge, and by employing the same numerical scheme and the same computational grid (potential–GFD). The computed potential field has been used to calculate the corresponding "no-Kutta" pressure field by using the following relation:

$$\hat{p}' = \bar{\rho}\,\bar{c}(ik\hat{\phi} - \bar{\mathbf{M}} \cdot \nabla\hat{\phi})$$

In this way the solution of the Lilley's equation can be interpreted as the solution of the problem with the Kutta condition, whereas the solution of the acoustic potential equation can be interpreted as the solution of the problem without the Kutta condition. A comparison between these two solutions, that are plotted in Fig. 6 along the line $y = 15$, clearly shows that the Kutta condition does not affect the phase of the diffracted wave. In fact, as shown by Fig. 6b, the zeros of the two solutions are coincident. On the contrary, as shown by Fig. 6a, the Kutta condition modifies the energy distribution, resulting in increased and decreased levels in the downstream and upstream radiation arcs, respectively.

C. Piecewise Constant Mean Flow

To make a step toward a realistic bypass duct configuration, the semi-infinite plate diffraction in the presence of a piecewise constant mean flow has been simulated. Results shown in this section are for an inner Mach number ($y < 10$) $\bar{M}_j = 0.5$ and an external Mach number $\bar{M}_0 = 0.3$. For this case the LEE–DGM solution has been used as a reference solution. Figure 7 shows a comparison between the two numerical solutions along the lines $y = 15$ and $y = 5$. It is evident that the Lilley–GFD results compare quite well with the LEE–DGM results. Some discrepancies occur only at an observation angle close to 110 deg along the line $y = 15$, where the relative L_0 error is about 10%. A nearly uniform phase error is also evident which is due to the different location of the effective edge in the two simulations.

In Fig. 8 results obtained by using the Lilley–GFD approach for the piecewise uniform flow case are superimposed to the results obtained for the uniform flow case. The velocity discontinuity causes

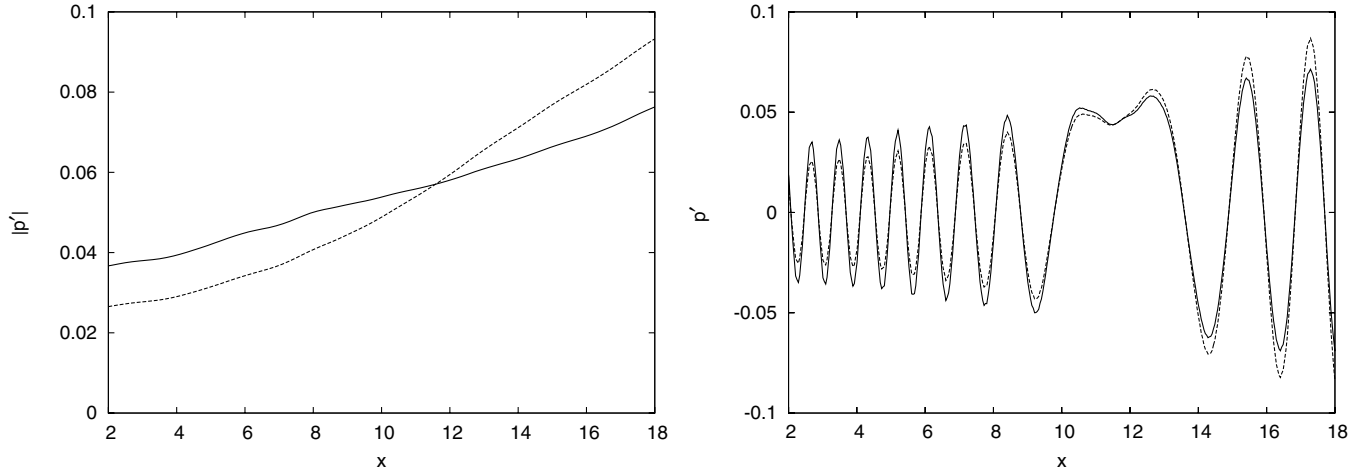

a) $|p'|$ **b)** $\mathrm{Re}(p')$

Fig. 6 Uniform flow case. Effect of the Kutta condition on the acoustic pressure along the line $y = 15$. Solid lines: potential-GFD (no-Kutta solution); dashed lines: Lilley–GFD (Kutta solution).

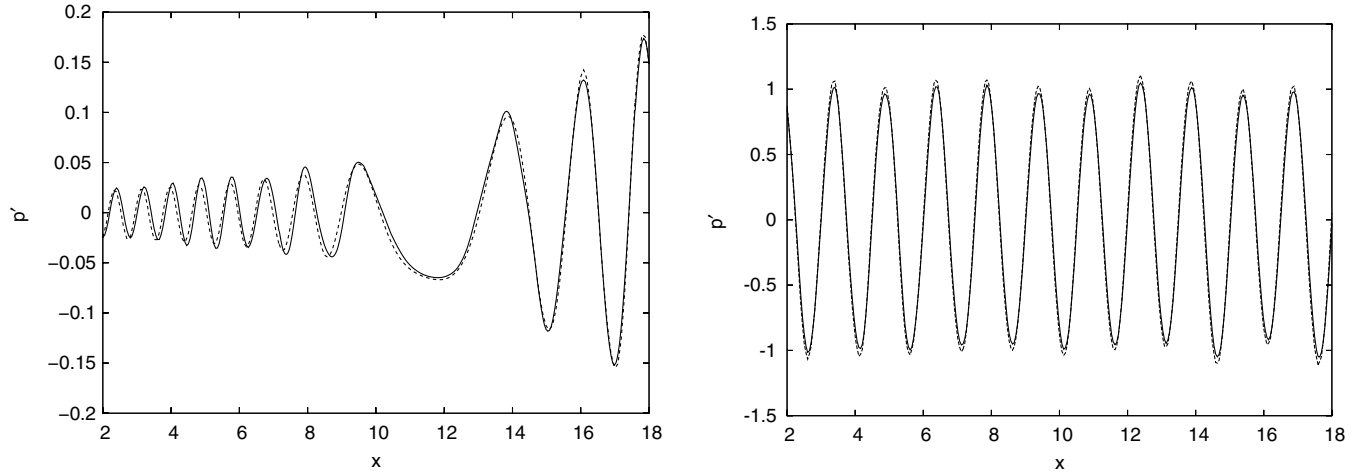

a) $y = 15$ **b)** $y = 5$

Fig. 7 Piecewise constant mean-flow case. Comparison between Lilley–GFD [$Re(p')$: solid lines] and LEE–DGM (p' at the start of a cycle: dashed lines) solutions.

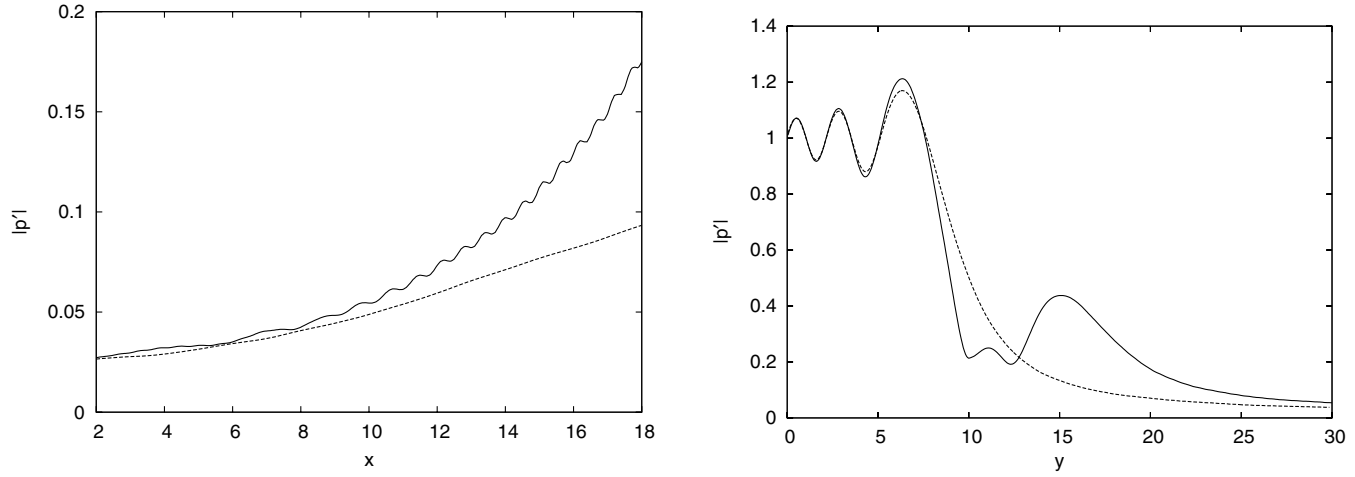

a) $|p'|$ **along** $y = 15$ **b)** $|p'|$ **along** $x = 28$

Fig. 8 Comparison between the pressure fields obtained by means of the Lilley–GFD method in the case of a piecewise constant flow (solid lines) and uniform flow (dashed lines).

an upward refraction of the acoustic energy and a consequent appearance of a silence zone. Figure 8a shows, in fact, that the flow discontinuity increases the acoustic levels downstream of the edge, whereas Fig. 8b shows that, in the case of a piecewise constant flow, the sound level does not decrease monotonically away from $y = 10$.

As a final remark, the oscillations in the magnitude of the acoustic pressure observed in Fig. 8a for the piecewise constant flow case are due to the fact that the radiation condition (16) provides a nonregular behavior at $y = 0$ due to the mean-flow discontinuity. As a consequence, spurious wave reflections are generated that interfere with the acoustic field.

D. Mixing Layer Mean Flow

The mean flow used in the previous section is a solution of the Euler system of equations because it is valid only in the limit of zero-diffusive effects. To take into account a more realistic mean flow, the mixing layer solution of the Navier–Stokes equations derived under the hypotheses of validity of the Prandtl mixing length model has been used [22]. The streamwise velocity distribution in a mixing layer between two streams of different Mach number is equal to

$$M(x, y) = \frac{\bar{M}_j + \bar{M}_0}{2}\left[1 - \frac{\bar{M}_j - \bar{M}_0}{\bar{M}_j + \bar{M}_0}\,\mathrm{erf}\left(\sigma\frac{y - y_E}{x - x_E}\right)\right] \qquad (17)$$

The corresponding temperature distribution can be deduced from the Crocco–Bouseman equation and the density from the equation of state, because the pressure is constant in the whole field. This solution is evidently self-similar, with the variable of self-similarity equal to $\sigma(y - y_E)/(x - x_E)$. The value $\sigma = 10$ of the mixing constant has been used in the present study, resulting in a mixing layer that at $x = 15$ has an extension comparable to the wavelength of the incident acoustic wave.

In Fig. 9 the results obtained with the Lilley–GFD and LEE–DGM approaches in the presence of a mixing layer are superimposed to the results obtained for the piecewise constant flow. The plots of the acoustic pressure along the line $x = 18$ show that the effect of the mixing layer is confined to its extension, thus resulting in a negligible influence on the outer field.

Finally, a comparison between the LEE–DGM and Lilley–GFD solutions is shown in Fig. 10. The acoustic pressure along the lines $y = 15$ and $y = 5$ exhibit a fairly good agreement. Significant discrepancies occur at an observation angle close to 90 deg along the line $y = 15$, where the relative L_0 error is about 10%. This includes both a numerical error and a modeling error due to the fact that the Lilley's equation and the LEE equations are not exactly equivalent in the presence of streamwise mean-flow gradients.

As an additional outcome of the present study, no instability waves have been observed, even if the acoustic wavelength is larger than the mixing layer thickness in the edge region. This is probably due to the

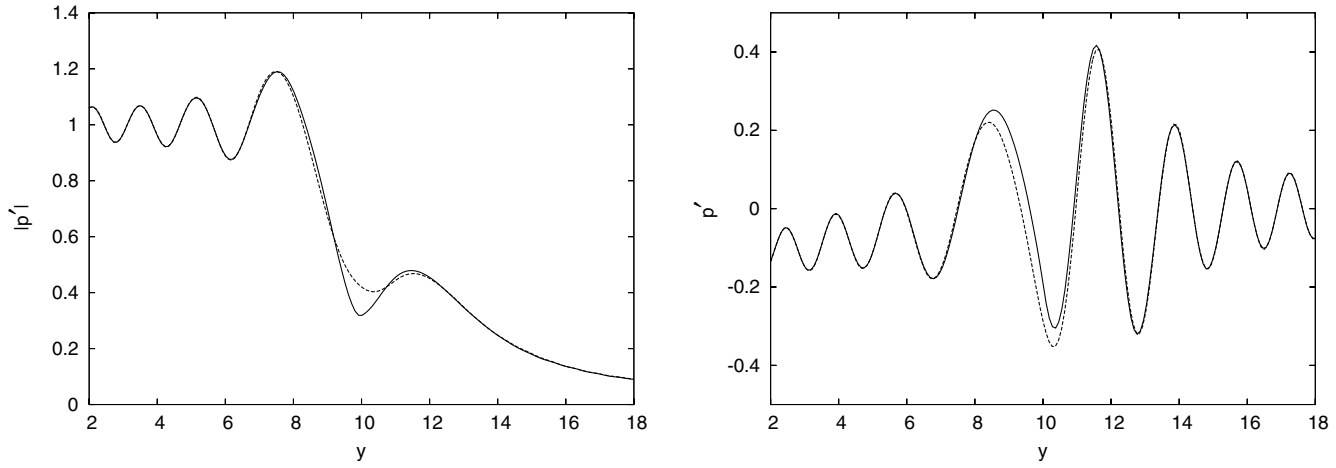

a) $|p'|$ (Lilley-GFD) **b) p' at the beginning of the cycle (LEE-DGM)**

Fig. 9 Mixing layer effect. Comparison between solutions obtained by using a piecewise constant flow (solid lines) and a mixing layer flow (dashed lines) along the line $x = 18$.

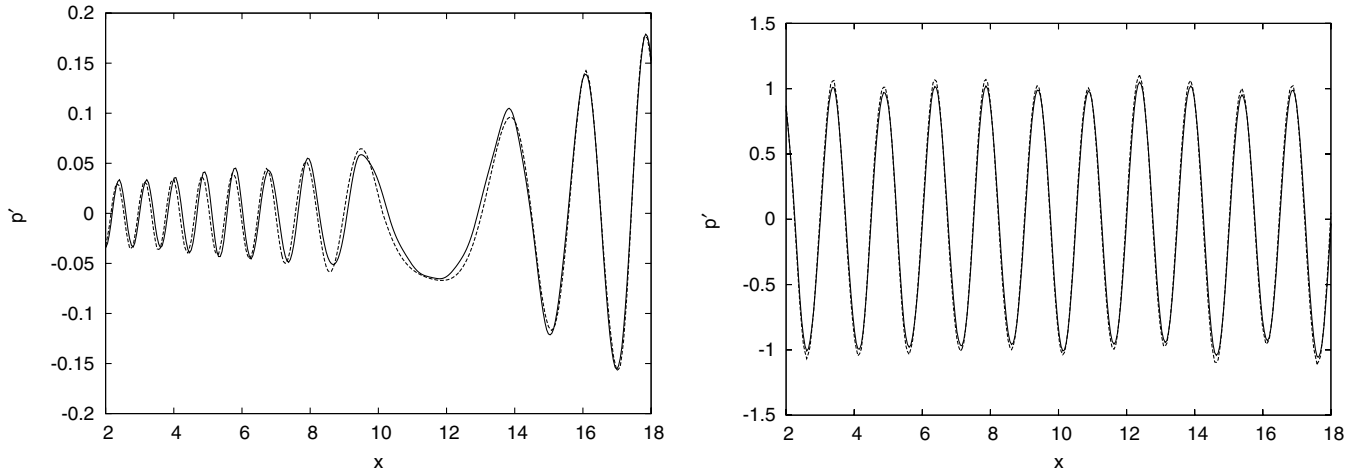

a) $y = 15$ **b) $y = 5$**

Fig. 10 Mixing layer mean-flow case. Comparison between Lilley–GFD [$Re(p')$: solid lines) and LEE-DGM (p' at the start of a cycle: dashed lines) solutions.

fact that the plate has zero thickness and consequently the mixing layer has zero initial thickness too. In fact, as pointed out in [23], the use of a shear layer with initial infinitesimal thickness restricts the band of unstable frequencies.

This concept is further supported by the fact that the solutions obtained through the Lilley–GFD approach by considering incident waves of different acoustic wave numbers ($k = 3.14$ and $k = 12.56$) are perfectly self-similar, as evident from Fig. 11. It can be therefore concluded that, for a zero-thickness plate and a plane wave parallel to it, the use of a mixing layer provides results that are very close to the ones obtained with a piecewise constant flow if the wavelength of the incident field is much larger than the plate and mixing layer thickness.

The main goal of this paper is to show that, in the case of a parallel shear flow, a scalar third-order wave equation is able to reproduce the solution of a complete linearized Euler system of equations, even if these two wave models are discretized in a very different way, and that these models provide, sufficiently far from the edge, the same results as those obtained analytically by Candel [10] for the half-plane Sommerfeld problem. Nevertheless, it is interesting to investigate the behavior of the Lilley–GFD solution near the edge at a distance much smaller than the acoustic wavelength. It is, in fact, well known that the pressure jump across the plate approaching the edge, say $x \to x_E^-$, behaves like $\sqrt{x_E - x}$. Numerical methods typically fail to capture this asymptotic behavior and require specific edge treatments. An opposite approach has been used in this paper. This consists of letting the method adapt itself to the edge by satisfying the wall boundary condition in the point upstream of the edge and the pressure-based wave equation in the point downstream. In this way it is not necessary to properly reconstruct the behavior at the edge but only near by. Figure 12 shows the asymptotic behavior of the pressure jump across the flat plate computed by interpolating the numerical solution in 2000 points along the lines $y = 10.001$ and 9.999 in the x interval (0, 20). The numerical behavior of $|p'_+ - p'_-|$ is compared with the curve $\sqrt{10.05 - x}$, evaluated at the same x coordinate of the numerical solution. Because of the small number of grid points per acoustic wavelength used to obtain the numerical solutions, the favorable agreement between the edge asymptotic behavior of the numerical solution and the theoretical behavior $\sqrt{x_E - x}$ is not a definitive proof of the capacity of the method to capture this asymptotic behavior, but only a starting point for a more detailed analysis.

The present verification study has demonstrated that the Lilley–GFD code is able to reproduce the correct solution of the Sommerfeld half-plane diffraction problem in the presence of a nonuniform flow because it solves a problem expressed in terms of pressure. Because

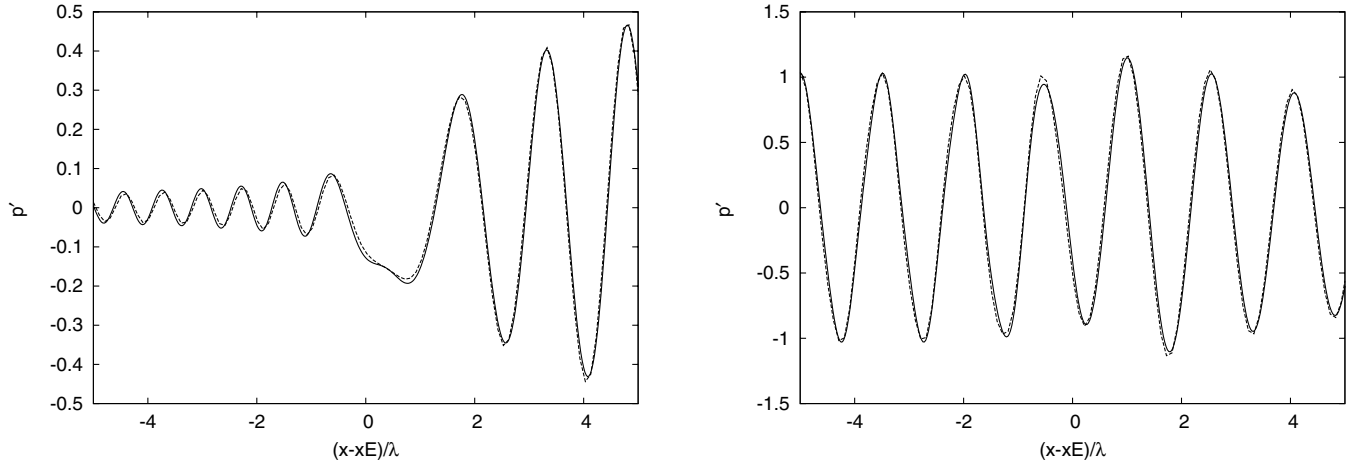

a) $\frac{y - y_E}{\lambda} = 1$ **b)** $\frac{y - y_E}{\lambda} = -1$

Fig. 11 Mixing layer mean-flow case. Effects of the frequency on the Lilley–GFD solution. Real part of the acoustic pressure for $k = 3.14$ (solid lines) and $k = 12.56$ (dashed lines). Coordinates referred to the acoustic wavelength λ.

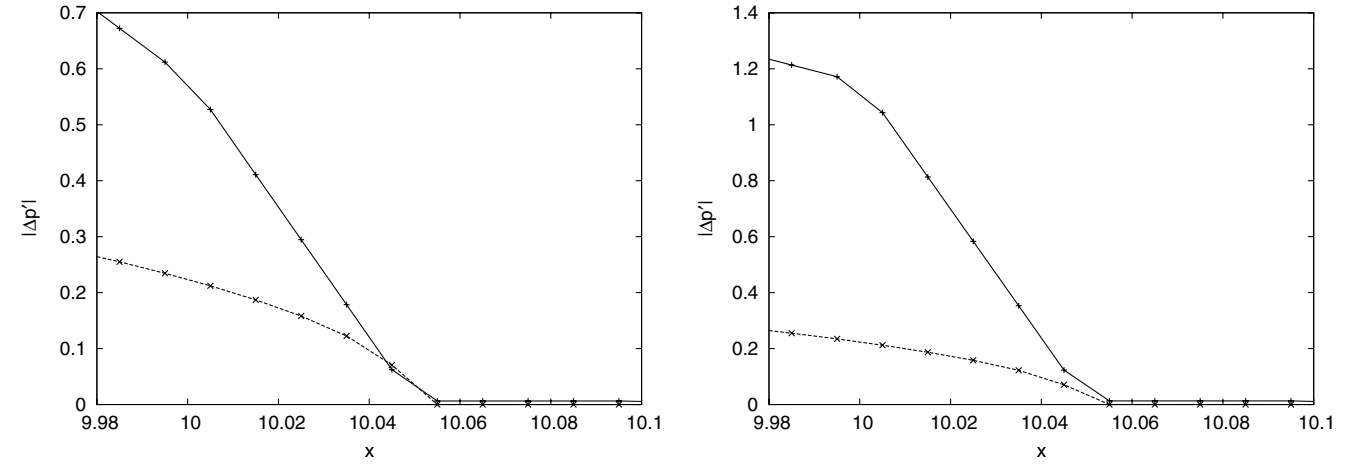

a) $k = 3.14$ **b)** $k = 12.56$

Fig. 12 Asymptotic behavior of the pressure jump across the plate obtained through the Lilley–GFD approach in the presence of a mixing layer. $|p'_+ - p'_-|$: solid lines; $\sqrt{10.05 - x}$: dashed lines.

the pressure fluctuation is continuous across the vortex sheet, the governing equation is valid also through it and therefore no explicit imposition of the pressure continuity is required. Hence, the edge no-modeling approach is the key point for the application of the Lilley–GFD method to an edge diffraction problem.

As an unexpected outcome of this study, the LEE–DGM code has demonstrated to be able to generate stable numerical solutions that support a nondiverging vortex sheet from the edge, as shown in Fig. 5. The proper Kutta behavior at the edge in this case is ensured by the fact that each grid cell communicates with the neighboring cells only via the fluxes at the boundaries. In fact, the continuity of the fluxes across the vortex sheet ensures the continuity of pressure and y-velocity fluctuations across $y = 0$, while enabling discontinuous x-velocity fluctuations. In other words, because the flow model is inviscid, the mechanism that permits one to generate the vorticity and satisfy the Kutta condition at the edge is numerical and not physical.

A final remark concerns the computational performances of Lilley–GFD and LEE–DGM codes. In the present work the Lilley's equation has been solved in the frequency domain, through a direct solution of the resulting linear system, thanks to the small number of discretization nodes, whereas the LEE equations have been solved in the time domain by using an explicit algorithm for the time integration. It is therefore obvious that, on one side, the CPU time may be dramatically affected by the core memory constraints that force one to use iterative linear system solvers for significantly large discretized problems, and on the other side, due to Courant number (CFL) constraints, the time integration may require long computations before reaching a periodic state throughout the computational domain. For these reasons a comparative CPU-time assessment of these two methods may be meaningful only in the case that also the LEE equations are discretized in the frequency domain. Reference CPU-time figures for both methods can be, however, provided by considering that, using one processor of a NEC TX-7 system, the Lilley–GFD simulation of the mixing layer case has required about 3 min, whereas the LEE–DGM simulation (third order in space and time, CFL $= 0.01$) has required about 30 h.

VI. Conclusions

In the present paper a numerical approach for the prediction of sound waves propagating through a nonuniform flow in the presence of a diffracting edge has been presented. The method is based on the solution of the linearized Lilley's equation in the frequency domain by using a GFD scheme. This approach seems to be a cheaper alternative to the solution of the complete set of linearized Euler equations. In addition the use of an equation written in terms of acoustic pressure avoid the explicit modeling of the vorticity shed from the trailing edge of the plate. This represents a clear advantage with respect to the solution of an acoustic potential wave equation. Moreover, the linearized Lilley's equation is also valid in the case of rotational mean flows that cannot be tackled by solving the potential wave equation. To comply with the analytical methods that have been developed under the low-frequency approximation, only results for a semi-infinite flat plate with zero thickness have been presented. The numerical results are in close agreement with the analytical solutions available in the literature and with numerical results obtained by solving the linearized Euler equations using a discontinuous Galerkin method.

References

[1] Redonnet, S., Manoha, E., and Kenning, O., "Numerical Simulation of the Downstream Fan Noise of 3D Coaxial Engines," AIAA Paper 2005-2816, 2005.

[2] Ewert, R., and Schröder, W., "On the Simulation of Trailing Edge Noise with a Hybrid LES/APE Method," *Journal of Sound and Vibration*, Vol. 270, No. 3, 2004, pp. 509–524. doi:10.1016/j.jsv.2003.09.047

[3] Ewert, R., "CAA Slat Noise Studies Applying Stochastic Sound Sources Based On Solenoidal Digital Filters," AIAA Paper 2005-2862, 2005.

[4] Sommerfeld, A., *Optics: Lectures on Theorethical Physics*, Vol. 4, Academic Press, New York, 1950.

[5] Noble, B., *Methods Based on the Wiener Hopf Technique*, Pergamon, New York, 1958.

[6] Bailly, C., and Juvé, D., "Numerical Solution of Acoustic Propagation Using Linearized Euler Equations," *AIAA Journal*, Vol. 38, No. 1, 2000, pp. 22–29.

[7] Rienstra, S. W., "Sound Diffraction at a Trailing Edge," *Journal of Fluid Mechanics*, Vol. 108, 1981, pp. 443–460. doi:10.1017/S0022112081002206

[8] Rawlins, B., "Diffraction by a Half Plane in a Moving Fluid," *Quarterly Journal of Mechanics and Applied Mathematics*, Vol. 58, No. 3, 2005, pp. 459–479. doi:10.1093/qjmam/hbi021

[9] Munt, R., "The Interaction of Sound with a Subsonic Jet Issuing from a Semi-Infinite Cylindrical Pipe," *Journal of Fluid Mechanics*, Vol. 83, 1977, pp. 609–640. doi:10.1017/S0022112077001384

[10] Candel, S. M., "Diffraction of a Plane Wave by a Half Plane in a Subsonic and Supersonic Medium," *Journal of the Acoustical Society of America*, Vol. 54, No. 4, 1973, pp. 1008–1016. doi:10.1121/1.1914311

[11] Casalino, D., and Bodony, D., "Green's Function Discretization of Pridmore-Brown Wave Operator," *Proceedings of the Summer Program 2006*, Center for Turbulence Research, Stanford Univ., Stanford, CA, 2006, pp. 547–558.

[12] Colonius, T., Lele, S. K., and Moin, P., "Sound Generation in a Mixing Layer," *Journal of Fluid Mechanics*, Vol. 330, 1997, pp. 375–409. doi:10.1017/S0022112096003928

[13] Bogey, C., Bailly, C., and Juvé, D., "Computation of Flow Noise Using Source Terms in Linearized Euler's Equations," *AIAA Journal*, Vol. 40, No. 2, 2002, pp. 235–243.

[14] Khavaran, A., and Bridges, J., "Modelling of Turbulence Generated Noise in Jets," AIAA Paper 2004-2983, 2004.

[15] Di Francescantonio, P., and Casalino, D., "Green's Function Discretization Scheme for Sound Propagation in Nonuniform Flows," *AIAA Journal*, Vol. 37, No. 10, 1999, pp. 1161–1172.

[16] Casalino, D., Roger, M., and Jacob, M., "Prediction of Sound Propagation in Ducted Potential Flows Using Green's Function Discretization," *AIAA Journal*, Vol. 42, No. 4, 2004, pp. 736–744.

[17] Casalino, D., and Genito, M., "Solution of a Linearized Lilleys Equation in the Frequency Domain for Turbofan Aft Noise Simulation," AIAA Paper 2007-3705, May 2007.

[18] Gabard, G., and Astley, R. J., "Theoretical Model for Sound Radiation from Annular Jet Pipes: Far- and Near-Field Solutions," *Journal of Fluid Mechanics*, Vol. 549, 2006, pp. 315–341. doi:10.1017/S0022112005008037

[19] Lilley, G. M., "On the Noise from Jets," CP-131, AGARD, 1974.

[20] Atkins, H. L., and Shu, C.-W., "Quadrature-Free Implementation of Discontinuous Galerkin Method for Hyperbolic Equations," *AIAA Journal*, Vol. 36, No. 5, 1998, pp. 775–782.

[21] Atkins, H. L., "Continued Development of the Discontinuous Galerkin Method for Computational Aeroacoustic Application," AIAA Paper 97-581, 1997.

[22] Batchelor, G. K., *An Introduction to Fluid Dynamics*, Cambridge Univ. Press, Cambridge, England, U.K., 1967.

[23] Barone, M. F., and Lele, S. K., "Receptivity of the Compressible Mixing Layer," *Journal of Fluid Mechanics*, Vol. 540, 2005, pp. 301–335. doi:10.1017/S0022112005005884

C. Bailly
Associate Editor